ChemistryEurope

ChemistryEurope
Excellence in Chemistry Research Worldwide

RESEARCH ARTICLE OPEN ACCESS

Hydration of Phenylium: Oxonium or Carbenium Ion Formation?

Corentin Rossi[1] | Anne P. Rasmussen[1,2] | Jean-Christophe Loison[3] | Bérenger Gans[1] | Laura Finazzi[4] | Jos Oomens[4] | Giel Berden[4] | Roland Thissen[5,6] | Nandana Pattathadathil[5,7] | Christian Alcaraz[5,6] | Ugo Jacovella[1]

[1]CNRS, Institut des Sciences Moléculaires d'Orsay, Université Paris-Saclay, Orsay, France | [2]CNRS, Bordeaux, INP, ISM, UMR 5255, Université Bordeaux, Talence, France | [3]Department of Physics and Astronomy, Aarhus University, Aarhus C, Denmark | [4]CNRS, Institut de Chimie Physique, UMR 8000, Université Paris-Saclay, Orsay, France | [5]Institute for Molecules and Materials, FELIX Laboratory, Radboud University, Nijmegen, The Netherlands | [6]Synchrotron SOLEIL, L'Orme des Merisiers, Gif-sur-Yvette, France | [7]Department of Physics, University of Trento, Trento, Italy

Correspondence: Ugo Jacovella (ugo.jacovella@cnrs.fr)

Received: 5 December 2025 | **Revised:** 2 February 2026 | **Accepted:** 5 February 2026

Keywords: gas-phase reactions | IR spectroscopy | isomers | kinetics | mass spectrometry

ABSTRACT

The hydration of the phenylium ion ($C_6H_5^+$) is investigated to determine whether the most abundant product structure is best described as an oxonium (O-protonated phenol) or carbenium (ring-protonated phenol) ion. Using a combination of infrared multiple-photon dissociation spectroscopy at the FELIX facility, collision-induced dissociation experiments, and quantum chemical calculations, we have characterized the reaction products formed upon the addition of water to phenylium. The IR fingerprint of the hydrated ion reveals dominant spectral features consistent with carbenium isomers, particularly the *ortho* and *para* forms, rather than the oxonium isomer. Reactivity measurements and branching ratios of the reaction between water and $C_6H_5^+$ produced by vacuum ultraviolet (VUV) dissociative photoionization of nitrobenzene at the SOLEIL synchrotron facility, as a function of internal energy show that protonated phenol forms efficiently in the gas phase. Computational modeling of the potential energy surface supports the preferential formation of carbenium structures and maps the key isomerization and dissociation pathways.

1 | Introduction

Phenylium (c-$C_6H_5^+$, m/z 77) is a well-known intermediate in both astrochemical aromatic chemistry and mass spectrometry. In mass spectrometry, it is widely formed from a variety of aromatic precursors through electron or chemical ionization. Its pronounced reactivity comes from its bivalency, exhibiting features of both carbenium (trivalent carbon) and carbene (divalent carbon) species. This dual character allows the phenylium to interact efficiently with both the σ- and π-electron systems. As a result, the ion at m/z 95—corresponding to the water adduct of phenylium—is a classic and routinely observed feature in mass spectrometry. This peak appears consistently in spectra acquired on commercial instruments, which typically operate under pressures that retain a significant background level of water vapor.

The water adduct of phenylium initially forms protonated phenol, the proton located on the oxygen atom, yielding an oxonium species (Oxo-). Subsequently, the proton can migrate to the phenyl ring, leading to different arenium ion isomers. The most stable structure corresponds to protonation at the *para* (p-) position. A slightly less stable isomer features protonation at the *ortho* (o-) position. In contrast, protonation at the *meta* (m-) or *ipso* positions is significantly less stable, as calculated by Solcà and Dopfer [1] and confirmed in the present work. Figure 1 presents these structures.

Phenol serves as the chromophore of the amino acid tyrosine, making it a valuable model for exploring hydrogen bonding in biological systems [2]. As a result, its solvation by water has been extensively studied [3–6] as a fundamental step toward understanding solute–solvent interactions. It has been shown that

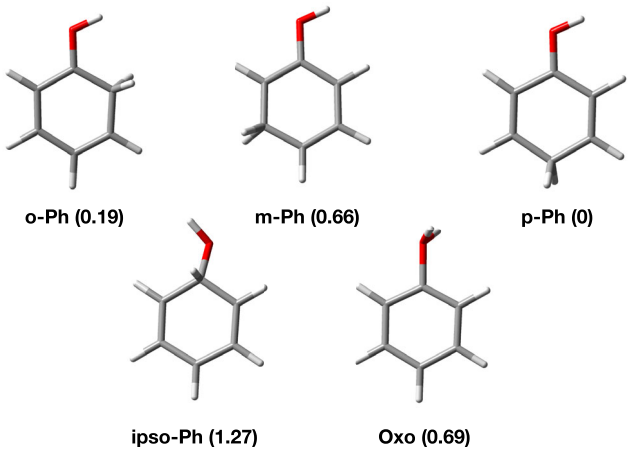

FIGURE 1 | The five structures of protonated phenol, along with their relative energies (in eV) with respect to the p-Ph, calculated at the M06-2X/cc-pVTZ level of theory.

protonation occurs predominantly on the oxygen atom in aqueous solution, whereas in the gas phase it preferentially takes place on the aromatic ring, highlighting the crucial role of the solvent environment in determining the site of protonation [7].

The groups of Dopfer and Fujii have spectroscopically investigated the structure of protonated phenol and its clusters, using characteristic vibrational fingerprints in the CH and OH stretching regions [1, 5, 8, 9]. In both studies, protonated phenol was generated via electric discharge in a supersonic expansion. Their results consistently revealed the coexistence of two distinct isomeric forms: the oxonium-type (**Oxo-type**) and species protonated at the para and/or ortho positions of the aromatic ring. In the following, we refer to all isomers where the protonation site is on the phenyl ring as **Carb-type** (for carbenium).

Interestingly, when phenol is protonated by CH_5^+ or H^+ under high-pressure conditions (0.5 to 500 mbar), the reaction appears to exclusively produce the global minimum structure, the para isomer or at least **Carb-type** species [10, 11]. This assignment is supported by collision-induced dissociation (CID) experiments using isotopic labeling and comparisons between experimental and theoretical hydration energies.

All of the aforementioned studies have used phenol as a precursor. Naturally, this raises the question whether similar results hold when starting instead from the ion-molecule reaction between phenylium and water. Surprisingly, only two studies have attempted to gain insight into the structure of the resulting product. In the study by Ranasinghe and Glish [12], phenylium reacted in a reaction cell containing a He/water mixture at a pressure of 3×10^{-4} mbar. CID analysis revealed a branching ratio of 90:10 for the loss H_2O versus the loss of CO. The former pathway is believed to indicate the formation of an **Oxo-type** structure, while the latter suggests a **Carb-type** structure. In a more recent study by Elroby et al. [6], they investigated the formation of the oxonium protonated phenol in the stepwise hydration of the phenyl cation in the gas phase without discussing why they excluded the **Carb-type** structures from their analysis.

Here, we explore for the first time the fingerprint region of protonated phenol using the free-electron laser FELIX combined with CID analysis. Additionally, we report for the first time the reaction cross section for the reaction between phenylium and water, and we investigate the influence of ion internal energy on the reactivity and branching ratios of the resulting products. The experimental results are supported by quantum chemical calculations.

2 | Experimental Setup

2.1 | Infrared Spectroscopy

The $C_6H_5^+$ ions were generated by injecting a solution of benzonitrile (Sigma-Aldrich) diluted in methanol with 1% of formic acid into an electrospray ionization (ESI) source. The resulting protonated benzonitrile was isolated in the ion trap and subsequently activated by CID to produce the fragment ion at m/z 77, which readily reacts with water to form protonated phenol species at m/z 95 [13]. IR spectra of protonated phenol were obtained using gas-phase action spectroscopy at the FELIX facility, Radboud University, Nijmegen, The Netherlands. The experiments employed a modified Bruker Amazon quadrupole ion trap mass spectrometer, allowing IR radiation from FELIX [14] to interact with trapped ions (see Martens et al. [15] for details). Briefly, after ESI at a flow rate of 120 µL/h, ions enter the vacuum of the mass spectrometer through a capillary and are trapped in the radio-frequency Paul-type ion trap. Ions of interest are mass-isolated and irradiated with 3 - 10 FELIX macropulses of up to 140 mJ at 10 Hz repetition rate. Fragmentation mass spectra after irradiation are averaged five times. To record IR spectra of CID fragment ions, mass-isolated precursor ions were fragmented using CID and fragment ions of interest were mass-isolated and then irradiated in an MS^3 stage. IR spectra were generated by plotting the fragment fluence as function of laser frequency. The laser is calibrated with a grating spectrometer with an accuracy of ±0.01 µm and the fragment fluence is corrected linearly for variations in FELIX power over the spectral range [16].

2.2 | Ion–Molecule Reactivity

Parent ions were generated by dissociative photoionization of nitrobenzene (Sigma-Aldrich) using vacuum ultraviolet (VUV) light in the 11–15 eV range at the DESIRS beamline of the SOLEIL synchrotron (Saint-Aubin, France). This method is well known to produce a pure sample of phenylium species [17, 18]. Reactions were studied with the CERISES setup, a home-built tandem mass spectrometer coupled to the VUV source [19, 20]. Parent ions were mass-selected, guided to the reaction cell with controlled collision energy, and product ions were analyzed by the second quadrupole. The typical timescale for an ion to travel from the source region to the reaction cell is approximately 80 µs. Absolute reaction cross sections were determined from the pressure of the neutral reactant (water) and ion counts, under single-collision conditions (pressure <100 nbar). The reaction with water was studied at fixed collision energy (0.05 eV in the center-of-mass frame) while varying the internal energy of the parent ions by tuning the photon energy.

2.3 | Quantum Chemical Calculations

To interpret the experimental observations on the reaction of $C_6H_5^+$ with H_2O, we performed DFT calculations of relevant

intermediates and transition states (TSs) using the M06-2X/cc-pVTZ level of theory. The highly nonlocal M06-2X functional, developed by Truhlar and coworkers [21], is particularly well suited for accurately describing the geometries and energetics of TSs [22].

3 | Results and Discussion

Figure 2 presents the reactivity of phenylium with water. The *y*-axis shows the reaction cross section (left) and the corresponding rate coefficient (right) as a function of the photon energy used to generate the phenylium ions. The internal energy of the $C_6H_5^+$ is directly related to the photon energy: specifically, the difference between the photon energy and the appearance energy (AE) of $C_6H_5^+$ represents the maximum internal energy that the phenylium ions can carry. The AE of phenylium derived from nitrobenzene has been investigated in several earlier studies [17, 23, 24]. Values reported by Panczel and Baer (11.14 eV) [23] and by Nishimura et al. (11.08 eV) [17] are slightly lower than the state-of-the-art value recommended by the Active Thermochemical Tables (ATcT) database [25] of 11.49 ± 0.02 eV at 300 K. In line with our recent study on the reactivity of phenylium with acetylene, we adopt the ATcT appearance energy as the most reliable reference. The major product is the water adduct at *m/z* 95 (shown in red), corresponding to protonated phenol. A minor product is also observed at *m/z* 94 (in blue), corresponding to the loss of a H atom from the water adduct. Both channels exhibit some energy dependence, peaking at low internal energy before decreasing and reaching a plateau. This behavior could also be influenced by isomeric effects, as other isomers of $C_6H_5^+$ are known to be significantly less reactive, as summarized by Loison et al. [18]. However, the observed change in reactivity occurs at internal energies below the expected isomerization barrier [26], likely too far to be accounted for even by kinetic shift effects. It appears that a clear discrimination between these two possibilities is not feasible, and that the dynamics of reactivity may arise from a combination of internal energy effects and changes in the isomeric population of the $C_6H_5^+$ species. The loss of CO from the water adduct (*m/z* 67), if it occurs at all, is extremely weak, below 0.1 Å^2.

Now that we have established, through quantitative analysis, that phenylium readily reacts with water, we turn to the question of the structure of the resulting water adduct, specifically, whether it is of **Carb-** or **Oxo-type**. To address this, we recorded the IR (IR multiple photon dissociation (IRMPD)) spectrum of the *m/z* 95 ion produced from the reaction of phenylium with water in a quadrupole ion trap. The spectrum was obtained by plotting the ion yield of all photofragments, normalized by the total ion count and further normalized by the photon flux, as a function of excitation wavelength. The experimental spectrum is shown in black in Figure 3, along with the predicted spectra of different protonated phenol isomers calculated using DFT methods.

The IRMPD spectrum was recorded over the 700–1900 cm^{-1} range. However, although all isomers are expected to exhibit distinct vibrational fingerprints below 1100 cm^{-1}, no significant bands were observed in this region of the experimental spectrum. This absence may be due to insufficient laser fluence at lower wavenumbers, preventing efficient multiphoton dissociation. Nevertheless, the simulated spectra for the Oxo and m-Ph isomers can confidently rule out these structures as the reaction product. The best, though not perfect, agreement is observed with the blue and green spectra corresponding to o-Ph and p-Ph, respectively. The key conclusion from Figure 3 is that the reaction product formed from the addition of water to phenylium is carbenium-type, since the two closest matching spectra correspond to **Carb-type** structures.

A common finding in the literature, as discussed in the Introduction, is the distinction between **Oxo-type** and **Carb-type** structures based on the nature of the fragment produced

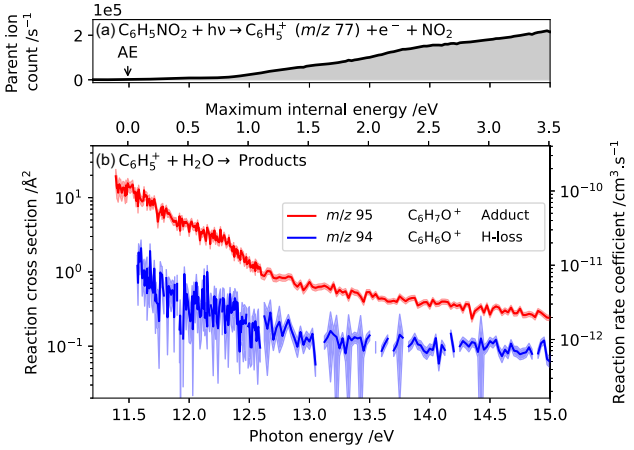

FIGURE 2 | Panel (a) displays the parent ion signal for the $C_6H_5^+$ ion obtained from dissociative ionization of nitrobenzene. The arrow indicates the appearance energy derived from the ATcT (11.49 eV). Panel (b) shows the reaction cross sections (left axis) and rate constants (right axis) with H_2O as a function of photon energy. Data points in the blue curve with an inconsistent error bar have been removed. The collision energy in the center-of-mass frame was set to 0.05 eV.

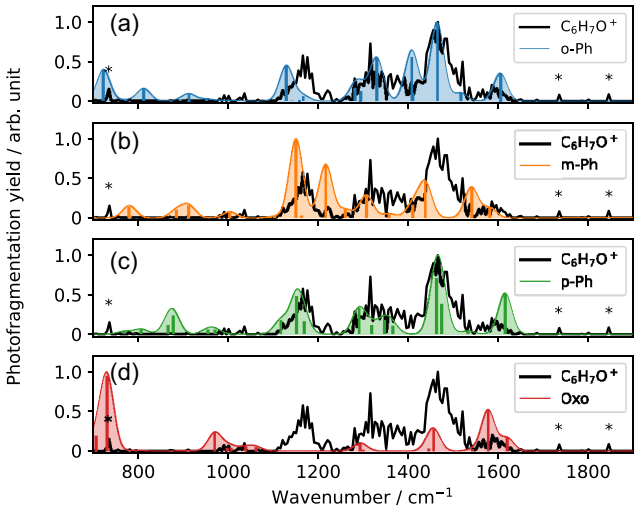

FIGURE 3 | Comparison between the experimental IR spectrum of protonated phenol (black solid line) and the scaled harmonic calculations for the singlet isomers o-Ph ((a), blue), m-Ph ((b), orange), p-Ph ((c), green), and Oxo ((d), red). The theoretical spectra were scaled by a factor of 0.965 [27] and convolved with a Gaussian function with a full width at half maximum (FWHM) of 35 cm^{-1}. Asterisks indicate artefactual features that should be disregarded.

by CID—specifically, CO loss for **Carb-type** and H_2O loss for **Oxo-type**. Therefore, we investigated the nature of the fragments generated by both photodissociation and CID, as shown in Figure 4. In both cases, three fragments are observed, corresponding to the loss of H_2O, CO, and [2C, 2H, O]. In the following discussion, we will focus exclusively on the losses of H_2O and CO. When fragmentation is induced using IR light, the relative abundance of the CO and H_2O loss varies by approximately a factor of two, depending on the specific vibrational transition targeted by the laser. In contrast, when fragmentation of protonated phenol is induced by collisions, the loss of CO dominates. This clearly indicates that the nature of the neutral loss is not a reliable indicator of the structure formed, as it is likely to depend strongly on the experimental conditions. Overall, our spectroscopic evidence supports the formation of predominantly the **Carb-type** structure, however, even in this case, approximately one-sixth of the fragments correspond to H_2O loss.

To further investigate why **Carb-type** structures predominantly result from the addition of water to phenylium, we computed key intermediates and TSs on the singlet potential energy surface (PES) of protonated phenol ($C_6H_7^+$). Energies were corrected for zero-point energy and a schematic representation of the surface is shown in Figure 5. The $C_6H_5H_2O^+$ adduct is connected to various **Carb-type** isomers via two TSs, both of which lie slightly below the energy of the $C_6H_5^+ + H_2O$ entrance channel. One TS leads to isomerization into *ipso*-Ph, the least stable of the **Carb-type** isomers, in agreement with the results reported by Solcà et al. [1]. Note that the ipso-Ph isomer is connected to the o-Ph isomer by a TS whose energy is below the energy of the *ipso* isomer after ZPE correction, which indicates that *ipso*-Ph most likely does not exist. The second TS corresponds to the isomerization of Oxo into o-Ph, a pathway not identified in the earlier study by Solcà et al.

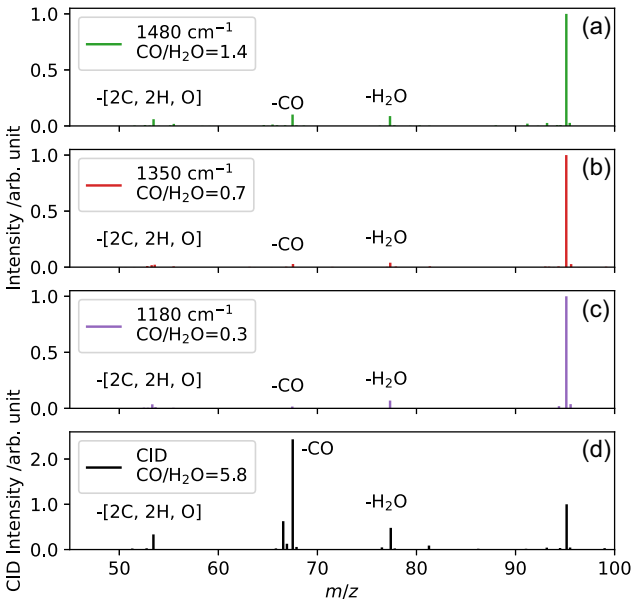

FIGURE 4 | Panels (a–c) show the mass spectra resulting from IR multiple photon dissociation (IRMPD) of protonated phenol at 1480, 1350, and 1180 cm^{-1}, respectively. Panel (d) displays a representative collision-induced dissociation (CID) spectrum of of protonated phenol acquired using the same instrument employed for the IR measurements and He as colliding partner.

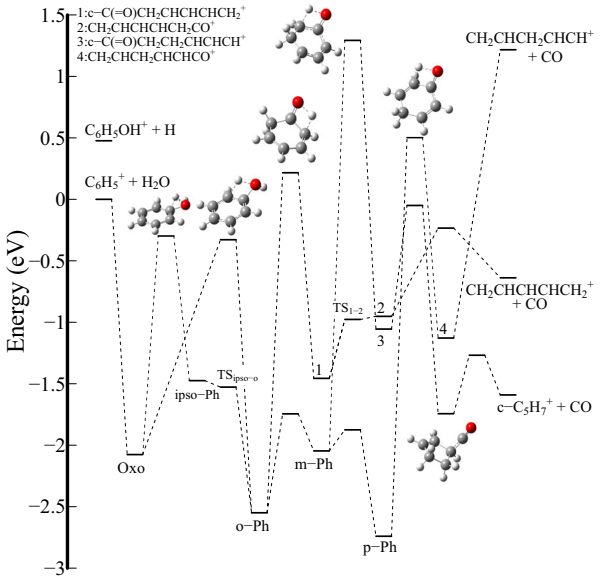

FIGURE 5 | Computed singlet potential energy surface (PES) connecting the principal isomers of protonated phenol and the most probable fragmentation pathways at the M06-2X/cc-pVTZ level of theory. All energies are given in eV relative to the p-Ph isomer.

After formation, the $C_6H_5OH_2^+$ adduct in its oxonium form possesses internal energy equal to its formation energy (2.13 eV). It can relax either through collisions or by radiative emission of IR photons. As noted by Herbst et al. [28], the typical timescales for isomeric conversion are much shorter than those for relaxation by collision or IR photon emission. Consequently, isomeric interconversion occurs rapidly compared to relaxation, leading to quasiequilibrated isomeric abundances (i.e., Oxo ⇄ o-Ph) at each internal energy.

The final isomer distribution is governed by the effective barriers to isomerization, corresponding to the energies of the relevant TSs. Under these conditions, the ratios between the isomeric forms can be approximated by the ratios of their rovibrational densities of states at the isomerization barriers. Once the water adduct is formed as an Oxo species, it can evolve either directly toward the o-Ph species or via the *ipso*-Ph intermediate, which lies in a shallow potential well without ZPE. Note that the energy required to reach the o-Ph structure is also sufficient to overcome the subsequent TSs leading to the global minimum, the p-Ph species. Using the Beyer-Swinehart algorithm, which provides estimates of the branching ratio, we find an Oxo/*ipso*-Ph ratio of 12 and an o-Ph/Oxo ratio of 3. These values provide additional qualitative support for the predominant formation of the **Carb-type** product, most likely in the o-Ph and p-Ph forms, as observed spectroscopically.

Carb-type isomers can further evolve to form $C_5H_7^+ + CO$, a transformation that requires migration of the hydrogen atom initially bound to oxygen onto the carbon ring. We identified several TSs enabling this hydrogen shift, all of which lie above the energy of the entrance channel ($C_6H_5^+ + H_2O$). We therefore also considered the competing loss pathways involving either H_2O or CO following infrared or collisional excitation. The loss of H_2O is more endothermic than CO loss but occurs without a barrier, making it the more favorable dissociation pathway.

In contrast, CO elimination is more challenging to rationalize, even at higher internal energies, since it involves multiple rearrangement steps, most notably the migration of the H atom from the OH group to the carbon ring. This migration constitutes the rate-limiting step, even when various $C_5H_7^+$ isomers are considered. The fragmentation channel leading to $C_6H_5OH^+ + H$ is observed in the reactivity experiments, with an onset a few hundred meV higher than adduct formation, in agreement with quantum chemical predictions. However, this channel is absent in dissociation processes induced by multiphoton excitation or CID experiments.

4 | Conclusion

This study demonstrates that the hydration of phenylium does not lead to a single dominant structure, but rather to a distribution of **Carb-type** isomers, composed of the *ortho* and *para* forms. IRMPD spectroscopy confirms that the reaction product is not an **Oxo-type** protonated phenol, but instead a ring-protonated species. While the loss of CO in CID and photodissociation experiments is clearly observed, our results show that the loss of CO or H_2O alone is not a reliable indicator of the underlying structure of protonated phenol. Overall, our findings elucidate the mechanistic details of the phenylium + water reaction and provide a framework for understanding the structure and reactivity of hydrated aromatic ions under isolated gas-phase conditions.

Author Contributions

Ugo Jacovella: investigation, conceptualization, writing – original draft, funding acquisition, supervision, project administration, **Corentin Rossi**: writing – review & editing, investigation, visualization, **Anne P. Rasmussen**: writing – review & editing, investigation, software, **Jean-Christophe Loison**: writing – review & editing, investigation, **Bérenger Gans**: writing – review & editing, investigation, **Laura Finazzi**: writing – review & editing, investigation, **Jos Oomens**: writing – review & editing, investigation, **Giel Berden**: writing – review & editing, investigation, **Roland Thissen**: writing – review & editing, investigation, **Nandana Pattathadathil**: writing – review & editing, investigation, **Christian Alcaraz**: writing – review & editing, investigation, **Ugo Jacovella**: writing – review & editing, investigation, conceptualization, funding acquisition, supervision, software.

Acknowledgments

The FELIX laboratory is supported by the Nederlandse Organisatie voor Wetenschappelijk Onderzoek (NWO). The work was funded by the French "Agence Nationale de la Recherche" (ANR) under grant no. ANR-22-CE29-0013 (Project iSELECTION). This work was also supported by a research grant (VIL71404) from VILLUM FONDEN.

Funding

This work was supported by Agence Nationale de la Recherche (22-CE29-0013), Nederlandse Organisatie voor Wetenschappelijk Onderzoek, Villum Fonden (VIL71404).

Conflicts of Interest

The authors declare no conflicts of interest.

Data Availability Statement

The data that support the findings of this study are available from the corresponding author upon reasonable request.

References

1. N. Solca and O. Dopfer, "Isomer-Selective Detection of Microsolvated Oxonium and Carbenium Ions of Protonated Phenol: Infrared Spectra of C6H7O+–Ln Clusters (L=Ar/N2, n≤6)," *The Journal of Chemical Physics* 120 (2004): 10470.

2. E. A. Meyer, R. K. Castellano, and F. Diederich, "Interactions with Aromatic Rings in Chemical and Biological Recognition," *Angewandte Chemie International Edition* 42 (2003): 1210.

3. M. Ataelahi and R. Omidyan, "Microhydration Effects on the Electronic Properties of Protonated Phenol: A Theoretical Study," *The Journal of Physical Chemistry A* 117 (2013): 12842.

4. H. Ishikawa, I. Kurusu, R. Yagi, R. Kato, and Y. Kasahara, "Quantitative Temperature Dependence of the Microscopic Hydration Structures Investigated by Ultraviolet Photodissociation Spectroscopy of Hydrated Phenol Cations," *The Journal of Physical Chemistry Letters* 8 (2017): 2541.

5. M. Katada and A. Fujii, "Infrared Spectroscopy of Protonated Phenol–Water Clusters," *The Journal of Physical Chemistry A* 122 (2018): 5822.

6. S. A. Elroby, S. G. Aziz, R. Hilal, I. K. Attah, S. P. Platt, and M. S. El-Shall, "Formation of the Oxonium Phenol Ion in the Stepwise Hydration of the Phenyl Cation in the Gas Phase," *Journal of Molecular Liquids* 322 (2021): 114541.

7. D. J. DeFrees, R. T. McIver Jr., and W. J. Hehre, "The Proton Affinities of Phenol," *Journal of the American Chemical Society* 99 (1977): 3853.

8. N. Solcà and O. Dopfer, "Protonation of Aromatic Molecules: Competition between ring and Oxygen Protonation of Phenol (Ph) Revealed by IR Spectra of PhH+–Ar," *Chemical Physics Letters* 342 (2001): 191.

9. N. Solcà and O. Dopfer, "Spectroscopic Identification of Oxonium and Carbenium Ions of Protonated Phenol in the Gas Phase: IR Spectra of Weakly Bound $C_6H_7O^+$–L Dimers (L = Ne, Ar, N_2)," *Journal of the American Chemical Society* 126 (2004): 1716.

10. K. Wood, D. Burinsky, D. Cameron, and R. Cooks, "Site of Gas-Phase Cation Attachment. Protonation, Methylation, and Ethylation of Aniline, Phenol, and Thiophenol," *The Journal of Organic Chemistry* 48 (1983): 5236.

11. L. J. Haupert and P. G. Wenthold, "Hydration Energies of Aromatic Ions in the Gas Phase," *The Journal of Physical Chemistry A* 117 (2013): 1164.

12. Y. A. Ranasinghe and G. L. Glish, "Reactions of the Phenylium Cation with Small Oxygen- and Nitrogen-Containing Molecules," *Journal of the American Society for Mass Spectrometry* 7 (1996): 473.

13. U. Jacovella, J. A. Noble, A. Guliani, et al., "Ultraviolet and Vacuum Ultraviolet Photo-Processing of Protonated Benzonitrile ($C_6H_5CNH^+$)," *Astronomy & Astrophysics* 657 (2022): A85.

14. D. Oepts, A. Van der Meer, and P. Van Amersfoort, "The Free-Electron-Laser User Facility FELIX," *Infrared Physics & Technology* 36 (1995): 297.

15. J. Martens, G. Berden, C. R. Gebhardt, and J. Oomens, "Cationization of Complex Anions in the Gas Phase: Structural and Thermodynamic Aspects," *The Review of Scientific Instruments* 87 (2016): 053104.

16. G. Berden, M. Derksen, K. J. Houthuijs, J. Martens, and J. Oomens, "An Automatic Variable Laser Attenuator for IRMPD Spectroscopy and Analysis of Power-Dependence in Fragmentation Spectra," *International Journal of Mass Spectrometry* 443 (2019): 1.

17. T. Nishimura, P. R. Das, and G. Meisels, "On the Dissociation Dynamics of Energy-Selected Nitrobenzene Ion," *The Journal of Chemical Physics* 84 (1986): 6190.

18. J.-C. Loison, C. Rossi, N. Solem, et al., "Evidence for Phenylium Reactivity under Interstellar Relevant Conditions," Under review at Nature Astronomy, available as arXiv:2506.13290 (2026).

19. B. Cunha de Miranda, C. Romanzin, S. Chefdeville, V. Vuitton, J. Žabka, M. Polášek, and C. Alcaraz, "Reactions of State-Selected Atomic Oxygen Ions O^+ (^{4}S, ^{2}D, ^{2}P) with Methane," *The Journal of Physical Chemistry A* 119 (2015): 6082.

20. C. Rossi, C. Alcaraz, R. Thissen, and U. Jacovella, "Tunable Photoionization Chemical Monitoring (TPI-CM)—A Means to Probe Molecular Ion Structures and Monitor Unimolecular Processes through Bimolecular Ion–molecule Reactions: Past, Present, and Future," *Journal of Physical Organic Chemistry* 36 (2023): e4489.

21. Y. Zhao and D. G. Truhlar, "The M06 Suite of Density Functionals for Main Group Thermochemistry, Thermochemical Kinetics, Noncovalent Interactions, Excited States, and Transition Elements: Two New Functionals and Systematic Testing of Four M06-Class Functionals and 12 other Functionals," *Theoretical Chemistry Accounts* 120 (2008): 215.

22. N. Q. Su, P. Pernot, X. Xu, and A. Savin, "When Does a Functional Correctly Describe Both the Structure and the Energy of the Transition State?," *Journal of Molecular Modeling* 23 (2017): 65.

23. M. Panczel and T. Baer, "A Photoelectron Photoion Coincidence (PEPICO) Study of Fragmentation Rates and Kinetic Energy Release Distributions in Nitrobenzene," *International Journal of Mass Spectrometry* 58 (1984): 43.

24. L. Cooper, L. Shpinkova, E. E. Rennie, D. Holland, and D. Shaw, "Time-of-Flight Mass Spectrometry Study of the Fragmentation of Valence Shell Ionised Nitrobenzene," *International Journal of Mass Spectrometry* 207 (2001): 223.

25. B. Ruscic and D. H. Bross, Active Thermochemical Tables (ATcT) Values Based on ver. 1.124 of the Thermochemical Network, Argonne National Laboratory, Lemont, Ill 2022, Accessed August 2023.

26. S. D. Wiersma, A. Candian, J. M. Bakker, et al., "IR Photofragmentation of the Phenyl Cation: Spectroscopy and Fragmentation Pathways," *Physical Chemistry Chemical Physics* 23 (2021): 4334.

27. D. Kashinski, G. Chase, R. Nelson, et al., "Harmonic Vibrational Frequencies: Approximate Global Scaling Factors for TPSS, M06, and M11 Functional Families Using Several Common Basis Sets," *The Journal of Physical Chemistry A* 121 (2017): 2265.

28. E. Herbst, R. Terzieva, and D. Talbi, "Calculations on the Rates, Mechanisms, and Interstellar Importance of the Reactions between C and NH2 and between N and CH2," *Monthly Notices of the Royal Astronomical Society* 311 (2000): 869.